Available online at www.sciencedirect.com

ScienceDirect

Energy Procedia 63 (2014) 5773 – 5786

Energy Procedia

GHGT-12

# First in-situ electrochemical measurement during fatigue testing of injection pipe steels to determine the reliability of a saline aquifer water CCS-site in the Northern German Basin

Anja Pfennig[a]*, Marcus Wolf[b], Katharina Heynert[a], Thomas Böllinghaus[b]

[a] *HTW University of Applied Sciences Berlin, Wilhelminenhofstraße 75 A, Gebäude C, 12459 Berlin, Germany*
[b] *BAM Federal Institute of Materials Research and Testing, Unter den Eichen 87, 12205 Berlin, Germany*

**Abstract**

During carbon dioxide storage technology (carbon capture and storage, CCS) components are exposed to a corrosive environment and mechanical stress, which results in corrosion fatigue and inevitably followed by the a lifetime reduction of these components. In order to gain knowledge upon the corrosion fatigue strength of materials, Samples of high alloyed stainless injection-pipe steels AISI 420 X46Cr13, and X5CrNiCuNb16-4 AISI 630 were tested in a at T=60 °C and ambient pressure in a $CO_2$-saturated synthetic aquifer environment similar to possible geological on-shore CCS-sites in the northern German Basin. Therefore a corrosion chamber applied to a resonant testing machine allowing for "in situ" test conditions was designed and successfully tested. In-situ tension compression experiments were established using a resonant testing machine at a frequency as low as 30 – 40 Hz. In addition technical $CO_2$ was introduced into the closed system at a rate close to 9 L/h to keep stable environmental conditions. Simultaneously electrochemical testing was performed to get information on failure causes and the mechanism of failure during the injection of $CO_2$ into deep geological layers. S-N plots, micrographic analysis, and surface analysis of the fracture surface were applied to obtain sustainable information on the corrosion fatigue behavior of injection pipe steels. Samples used have a surface roughness of Rz = 4, to simulate technically machined surfaces. X46Cr13 reached the maximum number of cycles ($12.5 \times 10^6$) at a stress amplitude of 173 MPa. X5CrNiCuNb16-4 reached the maximum number of cycles ($10 \times 10^6$) at a stress amplitude at 150 MPa. The scatter range of X5CrNiCuNb16-4 is very high (1:34); by comparison the scatter range of X46Cr13 is only 1:3.5.


Peer-review under responsibility of the Organizing Committee of GHGT-12

*Keywords:* steel; corrosion fatigue; electrochemistry; reliability; CCS; $CO_2$-storage

* Corresponding author. Tel.: +49 30 5019 4231; fax: +49 30 8104 3917.
*E-mail address:* anja.pfennig@htw-berlin.de


Peer-review under responsibility of the Organizing Committee of GHGT-12
doi:10.1016/j.egypro.2014.11.610

## 1. Introduction

The failure of pipe steels [1,2] during the engineering of a Carbon Capture and Storage (CCS) site [3], as found in the Northern German Basin, is caused during the compression of emission gasses from combustion processes. When injecting $CO_2$ into deep geological saline aquifer reservoirs (CCS Carbon Capture and Storage), the $CO_2$ is dissolved in the geological brine to build a corrosive environment. The anodic iron dissolution of the pipe steel results in the growth of a siderite corrosion layer ($FeCO_3$) on the alloy surface [4-7]. Corrosion processes will depend upon various sources, e.g. the injected gas, its composition and the presence of water and dissolved salts. Most likely at injection intervals, the aquifer water may flow back into the injection pipe and then form phase boundaries Here corrosion of the injection pipe in $CO_2$-rich aquifer water becomes likely [5,7]. The dependence also on environmental factors, such as the composition of surrounding media and alloy, temperature, $CO_2$ partial pressure, flow conditions, contaminations and formation of protective scales is mentioned in literature [4,18-20]. Two steels with differing allying elements appropriate for engineering a CCS site are analyzed applying a critical temperature of 60 °C well known for severe corrosion processes [3,5,7,21-26] .

An appropriate system for fatigue testing at temperatures existing in deep geological layers (in-situ conditions) was set up, to assess materials of components loaded cyclically and exposed constantly to the highly corrosive hot thermal water at 60 °C and ca. 20 % salinity of the geothermal water and fluid properties differing strongly [27]. The inevitably following corrosion fatigue reduces the lifetime of these components. Frequency, temperature and chloride concentration show strong influence on the corrosion processes with applied mechanical stress [28]. Corrosion fatigue mechanisms are enhanced, especially in steels with low chromium content [26] and in the presence of chlorides [29], hydrogen sulfide ($H_2S$) [30] as well as $CO_2$ [31]. The endurance limit will decrease with increasing temperature, increasing mechanical load and decreasing pH for high alloyed steels [33]. But increasing chromium content of steels as well as internal compressive stress in surface regions will increase the endurance limit [34]. To understand the influence of corrosive media on the mechanical behavior of stainless steels such as AISI 630 (X5CrNiCuNb16-4, 1.4542) and AISI 420 C (X46Cr13, 1.4034) especially during carbon capture and storage as well as in geothermal energy production the following results were obtained.

## 2. Material and Methods

### Exposure Tests

Exposure tests were carried out using samples of martensitic AISI 420C (X46Cr13, 1.4034), and AISI 630 (X5CrNiCuNb16-4, 1.4542) (table 1) with 8 mm thickness and 20 mm width and 50 mm length. A hole of 3.9 mm diameter was used for sample positioning. Heat treatment prior to exposure was done following routine protocols.

The surfaces were activated by grinding with SiC-Paper down to 120 µm under water. Samples of each base metal were positioned within the vapour phase (1 bar), the supercritical phase (100 bar) and within the liquid phase. The brine (as known to be similar to the Stuttgart Aquifer [20]: $Ca^{2+}$: 1760 mg/L, $K^{2+}$: 430 mg/L, $Mg^{2+}$: 1270 mg/L, $Na^{2+}$: 90,100 mg/L, $Cl^{-}$: 143,300 mg/L, $SO_4^{2-}$: 3600 mg/L, $HCO_3^{-}$: 40 mg/L) was synthesized in a strictly orderly way to avoid precipitation of salts and carbonates. The exposure of the samples between 700 h to 8000 h was disposed in a chamber kiln at 60 °C at 100 bar in an autoclave system and for reference at ambient pressure as well. Flow control (3 NL/h) at ambient pressure was done by a capillary meter GDX600_man by QCAL Messtechnik GmbH, München.

Table 1: Chemical composition of AISI 420C (X46Cr13, 1.403,) and AISI 630 (X5CrNiCuNb16-4, 1.4542).

| El [a] | **X5CrNiCuNb16-4** acc standard | **(1.4542)** analysed [b] | **X46Cr13** acc standard | **(1.4034)** analysed [b] |
|---|---|---|---|---|
| C | ≤ 0.07 | 0.03 | 0.42 - 0.5 | 0.46 |
| Si | ≤ 0.70 | 0.42 | < 1.00 | 0.25 |
| Mn | ≤ 1.50 | 0.68 | < 1.00 | 0.45 |
| P | ≤ 0.04 | 0.018 | < 0.045 | 0.018 |
| S | ≤ 0.015 | 0.002 | < 0.03 | 0.003 |
| Cr | 15.0 - 17.0 | 15.75 | 12.5 - 14.5 | 13.39 |
| Mo | ≤ 0.60 | 0.11 | | 0,.03 |
| Ni | 3.00 – 5.00 | 4.54 | | 0.13 |
| Co | | | | 0.03 |
| Cu | 3.00 – 5.00 | 3.00 | | |
| Nb | 0.20 – 0.45 | 0.242 | | |
| Fe | rest | 75.00 | rest | 85. 4 |

[a] elements as specified according to **DIN EN 10088-3 in %**
[b] spark emission spectrometry

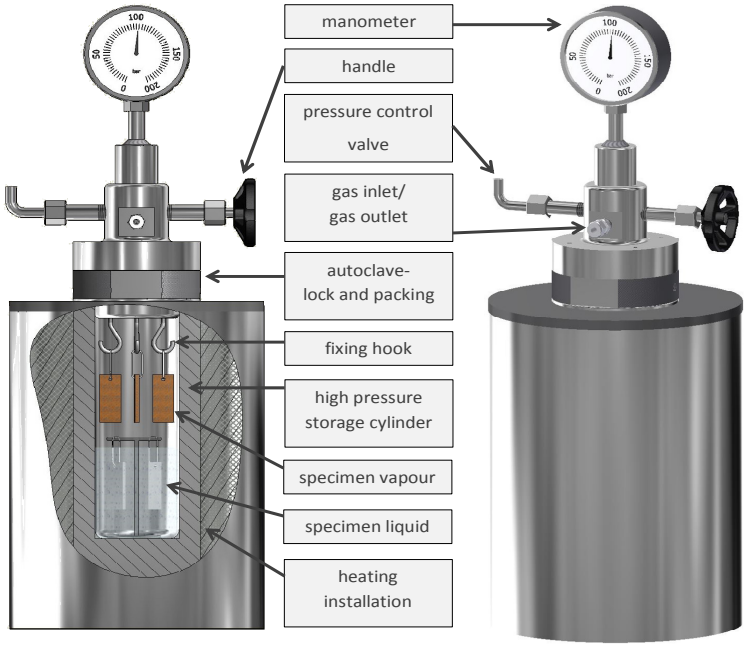


Fig. 1. Experimental set-up of laboratory corrosion experiment: autoclaves 100 bar/60 °C.

X-ray diffraction was carried out in a URD-6 (Seifert-FPM) with CoKα-radiation with an automatic slit adjustment, step 0.03 and count 5 sec and AUTOQUAN ® by Seifert FPM was used for phase analysis. For gravimetric measurement descaling of the samples (60°C/700 h, 2000 h, 4000 h, 8000 h) was performed by exposure to 37% HCl for 24 hours and mass gain was analyzed according to DIN 50 905 part 1-4. To characterise the pitting corrosion, 3-D-images were realized by the double optical system Microprof TTV by FRT. Non-descaled

parts of the samples were embedded in a cold resin (Epoxicure, Buehler), cut and polished first with SiC-Paper from 180 µm to 1200 µm under water and then finished with diamond paste 6 µm, 3 µm and 1 µm. The measurement of the layer thicknesses and residual pipe wall thicknesses as well as microstructure analysis were performed via light and electron microscopy techniques using the semi-automatic analyzing program Analysis Docu ax-4 by Aquinto. A set of 100 linescans was measured taking 10 to 20 micrographs per parameter.

**Fatigue Tests**

The objective was to simulate in-situ conditions (temperature 60 °C, corrosive environment) of a material exposed to dynamic mechanical stress and corrosive gas- saturated saline aquifer environment. The corrosion chamber is fixed directly onto the sample leaving the resonant testing machine unaffected (figure 2). During mechanical stress-strain tests a magnetically driven gear pump constantly pumps the corrosive media from the reservoir to the corrosion- and temperature-resistant corrosion chamber. The specimen is during the complete test surrounded of the corrosions medium. Heating is realized by a heating element witch is placed at the reservoir. The ratio of sample surface to volume of the corrosive media after DIN 50905 Part 1 (10 ml/cm²) is greater than required. The connecting of the chamber onto the specimen via clamping collar creates a force-fit process ensuring enough force to the corrosion chamber at high frequencies to keep it firmly on the test specimen. The corrosion chamber is sealed by O-rings made of Viton in the area of restraint. In order not to impede the change in length of the sample during the experiment, a membrane is applied to the corrosion chamber as a motion-compensating element.

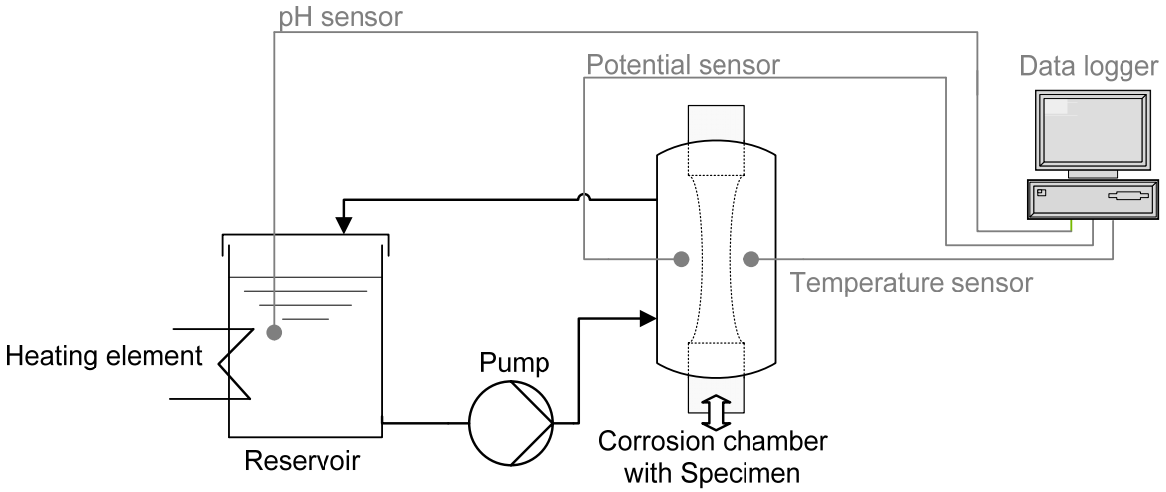


**Fig. 2: Schematic set-up of operating corrosion chamber for in-situ corrosion fatigue testing.**

The corrosion chamber is also equipped with measurement technique to obtain electrochemical data during the mechanical tests. There are sensors to measure the temperature, the pH and the electrochemical potential. For measurement of the electrochemical potential a special is used. The silver-silver chloride electrode is shock resistant and hence optimized for use inside the corrosion chamber under cyclically load. The silver wire is fixed in a channel made of Teflon.

Tests are performed in a resonance test machine with a frequency of 30~40 Hz.

**Electrochemical Reference Tests**

The experimental equipment is designed for electrochemical reference tests under the same conditions as realized in the corrosion chamber, but without mechanical stress (figure 3). The corrosion medium was pumped by a

flexible-tube pump from the reservoir into the measurement chamber. Heating is realized by a heating element fixed to the top of the reservoir. The measurement chamber is equipped with the same sensors and the same fitting system as the corrosion chamber to guarantee similar test conditions, such as: sensors to measure temperature, pH and electrochemical potential. The measurement chamber itself is made of PTFE to prevent influence of the camber material on the electrochemical potential.

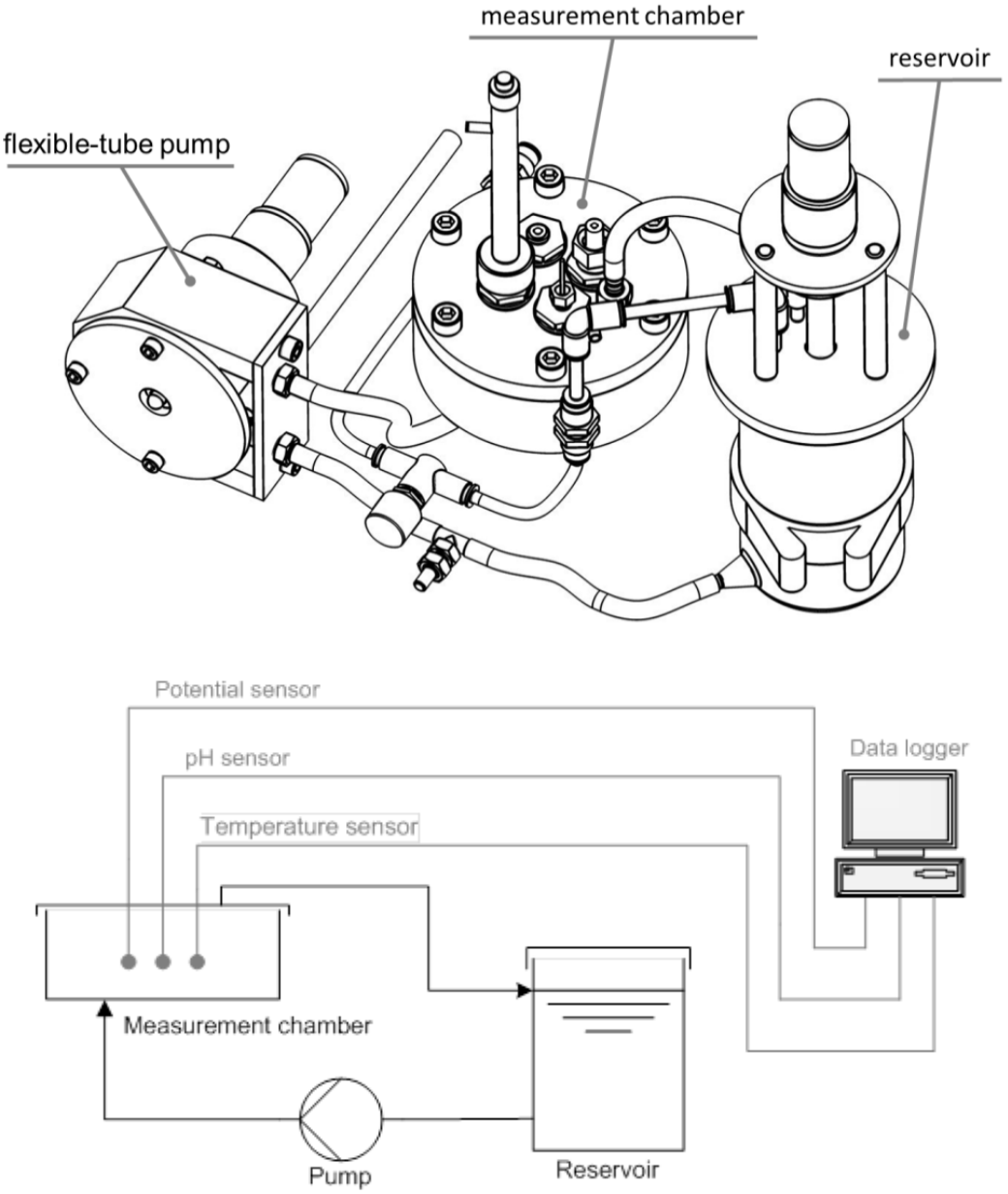


Fig. 3. Experimental and schematic set-up and of electrochemical reference tests.

## 3. Results and Discussion

### *3.1. Exposure Tests: Microstructure and Corrosion rates*

In the case of intermissions of the injection during carbon dioxide storage the water level may rise leading to the precipitation of corrosion products and formation of pits at the inner injection pipe surface. Therefore specimens kept in the liquid $CO_2$-saturated aquifer brine form a non-uniform carbonate layer differing in thickness but covering the entire surface as result of the low siderite $FeCO_3$-solubility in $CO_2$-containing water, because the resulting carbonic acid leads to low pH (figure 4).

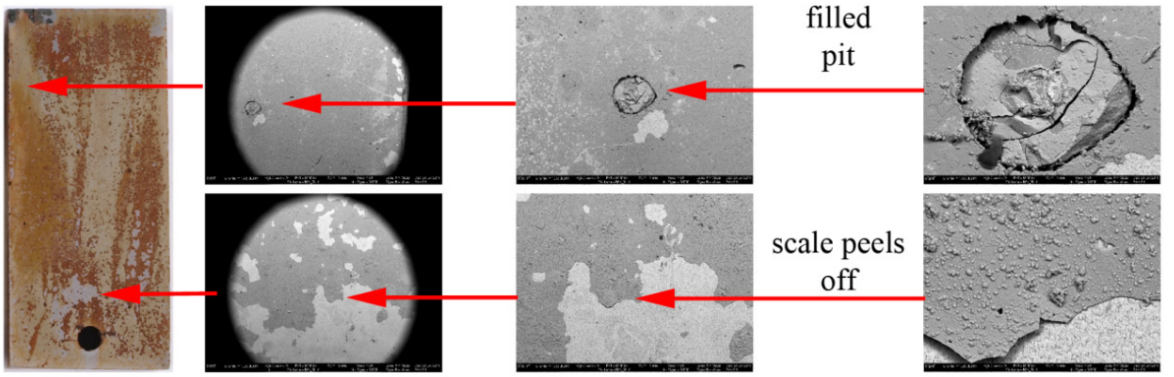


Fig. 4. Sample surfaces of X46Cr13 after 4000 hours of at 60 °C and 100 bar to $CO_2$-saturated aquifer water.

The multi-layered carbonate/oxide structure reveals siderite $FeCO_3$, goethite a-FeOOH at 100 bar and additionally mackinawite FeS and akaganeite $Fe_8O_8(OH)_8Cl_{1.34}$ as well as carbides, $Fe_3C$ and spinel-phases of various compositions at ambient pressure and is described in detail by Pfennig et al. [24,25]. The pit formation is driven by the formation of carbonic acid and existence of $HCO_3$. Pits are covered with corrosion products, mainly siderite as the main phase, that were found on the surface elsewhere [24,25]. At high pressure (100 bar) corrosion rates and scale thicknesses of X46Cr13 in $CO_2$ saturated geothermal brine obtained from static experiments, are generally lower than at ambient pressure. Surface corrosion rates are below 0.01 mm/year at 100 bar and about 0.05 mm/year at ambient pressure after 8000 h of exposure. Therefore it can be assumed that fatigue corrosion effects may be less sensitive to higher pressure.

In general X5CrNiCuNb16-4 reveals similar corrosion products as X46Cr13, but shows a discontinuous surface layer already after 1000 h of exposure at ambient pressure and even stronger at 100 bar growing more distinct the longer the exposure to $CO_2$-saturated aquifer water (figure 5). The reason for this unusual behaviour has not been solved yet, but it may be due to heterogeneous carbide distribution within the microstructure leading. Carbides are more susceptible to corrosion initiation [24] and therefore the passivation of the steel surface is locally reduced leading to homogeneous elliptical corrosion phenomena. This is one strong reason for the unusual corrosion fatigue behaviour as demonstrated further on.

X5CrNiCuNb16-4 with martensitic microstructure shows lowest corrosion rates around 0.002 mm/year at ambient pressure (figure 6). After normalizing samples corrode around 0.01 mm/year determined after 6000 hours of exposure. In the beginning of the corrosion process an increase of the corrosion rate after 1000 h of exposure is followed by a decrease for all samples until 4000 h of exposure. This incubation time results in a breakdown of the

passivation layer building up again after longer exposure but being not sufficient after more than 4000 h: after 4000 h of exposure the corrosion rates increase again.

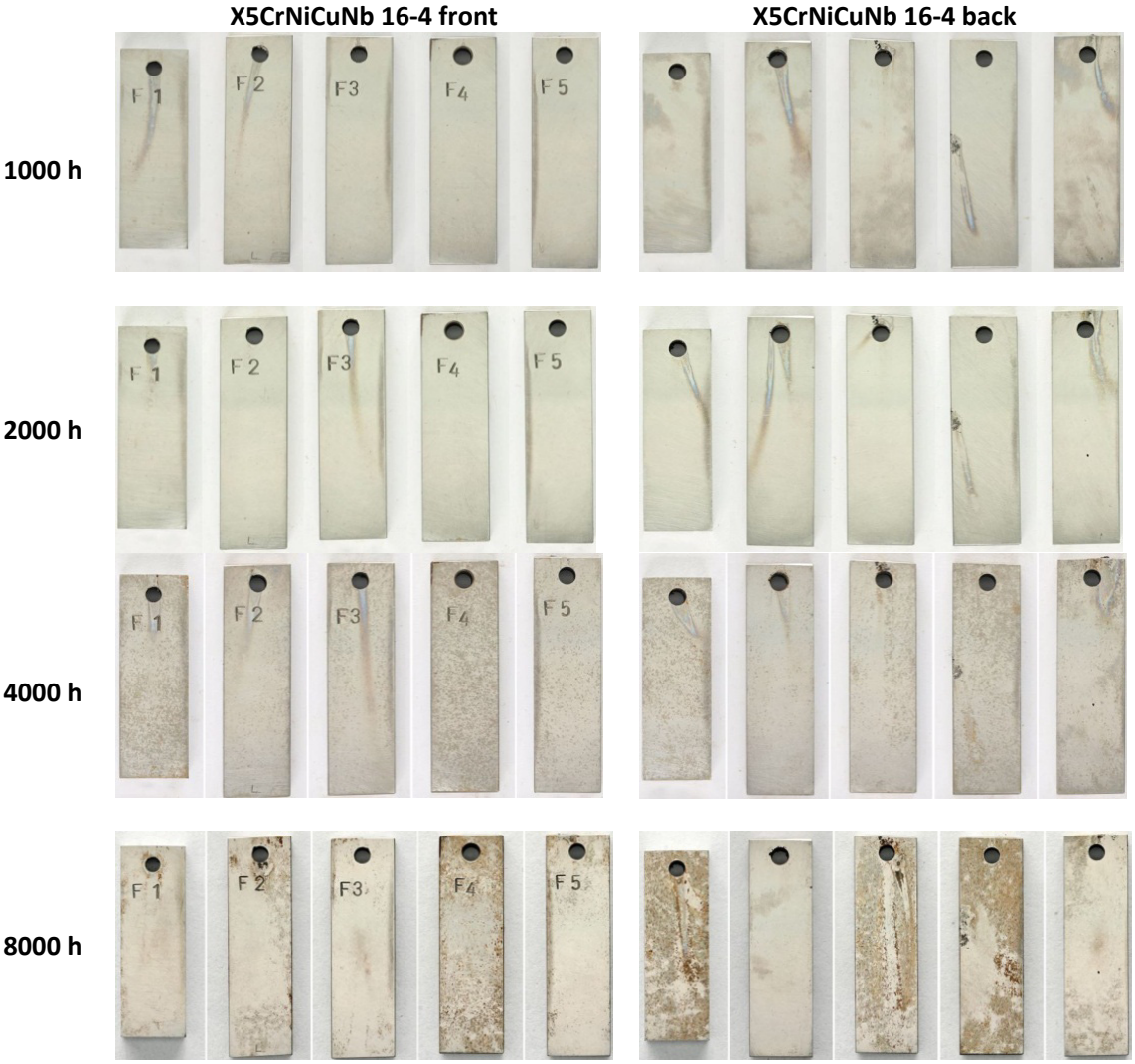


Fig. 5. Sample surfaces of differently heat treated X5CrNiCuNb16-4 after 1000 to 8000 hours of exposure to $CO_2$-saturated aquifer water at 60 °C and 100 bar. Heat treatment from left to right: normalizing, hardening at 1040 °C, hardening+tempering at 1040 °C + 550 °C, 650 °C and 755 °C

Due to sufficient thickness of the carbonate layer mutual diffusion of ionic species and growth of the corrosion layer is reduced, but at the same time pit growth is enhanced. Independent of the exposure time the least amount of pits is found on steels with martensitic microstructure. In general fewer pits are found on X46Cr13. Although the high amount of alloying elements preventing from corrosion X5CrNiCuNb16-4 has a rather high number of pits per $m^2$ regardless of heat treatment prior to exposure. Pit depths measured on X46Cr13 (8-25 µm) do not penetrate as deep as pits measured on X5CrNiCuNb16-4 (10-150 µm). Reliable corrosion rates and lifetime predictions regarding pit corrosion in CCS technology are not possible, because pit growth is a statistical phenomenon with little predictability and cannot be calculated as easily as surface corrosion rates.

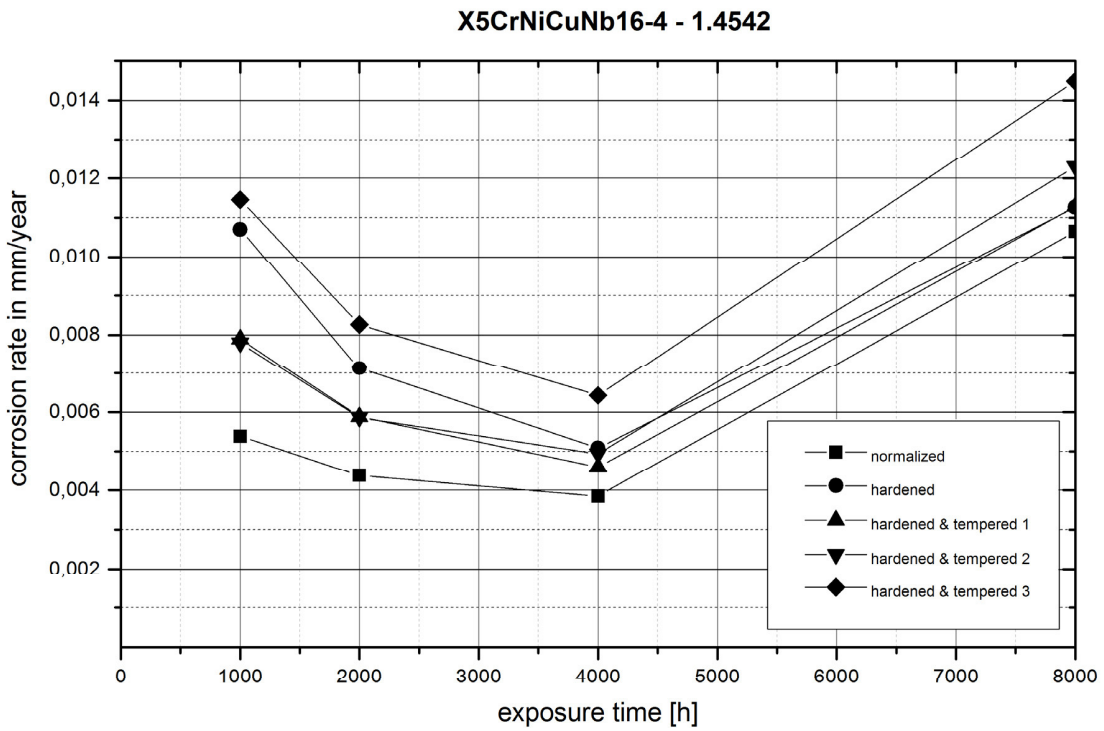


Fig. 6. Corrosion rate of X5CrNiCuNb16-4 after 8000 hours of exposure to $CO_2$-saturated aquifer brine water at 60 °C and 100 bar differently heat treated prior to exposure.

Due to sufficient thickness of the carbonate layer mutual diffusion of ionic species and growth of the corrosion layer is reduced, but at the same time pit growth is enhanced. Independent of the exposure time the least amount of pits is found on steels with martensitic microstructure. In general fewer pits are found on X46Cr13. Although the high amount of alloying elements preventing from corrosion X5CrNiCuNb16-4 has a rather high number of pits per $m^2$ regardless of heat treatment prior to exposure. Pit depths measured on X46Cr13 (8-25 µm) do not penetrate as deep as pits measured on X5CrNiCuNb16-4 (10-150 µm). Reliable corrosion rates and lifetime predictions regarding pit corrosion in CCS technology are not possible, because pit growth is a statistical phenomenon with little predictability and cannot be calculated as easily as surface corrosion rates.

### *3.2. Fatigue Tests: Endurance limit*

The corrosion fatigue strength of stainless steel with 13% chromium (X46Cr13, 1.4034) and 16% chromium (X5CrNiCuNb16-4, 1.4542, hardened and tempered with martensitic microstructure) is examined in dynamic stress-strain tests in $CO_2$-saturated aquifer (Stuttgart Aquifer [20]) at 60 °C. Therefore a resonant testing machine (sinusoidal dynamic test loads, R=-1; resonant frequency ~ 30 Hz) has been used. In addition technical $CO_2$ was introduced into the closed corrosion chamber system at a rate close to 9 L/h to keep stable environmental conditions. In each test series 30 specimens were tested. X46Cr13 was tested at stress amplitudes between 173 MPa and 270 MPa (figure 7) and X5CrNiCuNb16-4 between 150 MPa and 500 MPa (figure 8). Due to the rather heterogeneous fine machined surfaces (surface roughness Rz=4) the specimens are comparable with prefabricated parts.

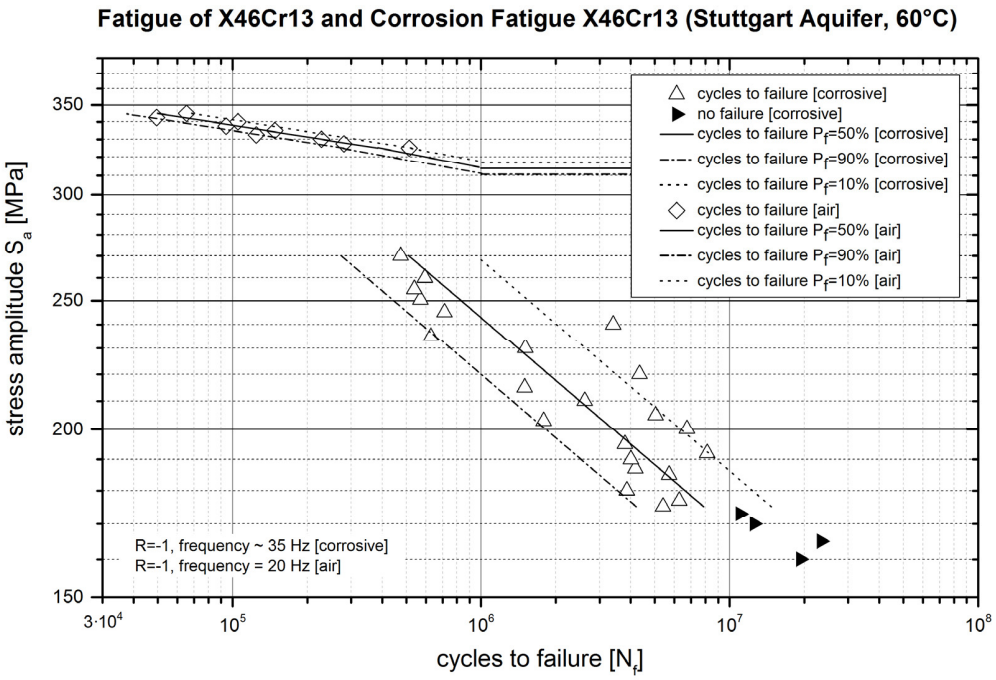


Fig. 7: S-N-curve of X46Cr13 tested in air and in the corrosion chamber, exposed to flowing saline aquifer [20] and $CO_2$.

Without corrosive environment the fatigue strength of X46Cr13 (theoretically an infinite number of load cycles without failure) shows a relatively smooth slope (figure 7). The maximum number of cycles (12.5 x $10^6$) at a stress amplitude of 173 MPa is reached, after test duration of $10^7$ cycles [33].

X5CrNiCuNb16-4 reached the maximum number of cycles (10 x $10^7$) at a stress amplitude of 150 MPa. The decrease of the fatigue limit line of 1.4542 samples with increasing number of cycles (Wöhler-exponent of k = 3.59) is much larger in corrosive environment than in air (tensile strength in air: 1078 MPa, largest number of cycles in corrosive environment (0.6 x $10^7$ at 200 MPa). Similar to 1.4034 [33] also 1.4542 shows no typical fatigue strength demonstrated in a log-log plot in figure 8. Ordering the number of failures within the S-N-plot results in groups of three (as demonstrated by different type of lines). This may be due to inhomogeneous microstructure such as element distribution or possibly different charges of aquifer water. But, the latter is rather unlikely, because the chemical analysis as well as procedure and chemical input have been kept stable throughout the entire test series. The unusual surface corrosion pattern as well as the unusual S-N plot demonstrates a distinct corrosion behavior influencing mechanical performance under corrosive environment. The coefficient of correlation $r^2$ = 0.33 from the regression is unusually small so that the hypothesis of a (linear) relationship of the considered variables is doubted. In addition, the scattering range TN = 1:34.4 is disproportionately large compared to the scatter range of X46Cr13 of only 1:4. The corrosion fatigue strength of X46Cr13 is approx. 36% below the endurance limit measured in air. X5CrNiCuNb16-4 is 60% below the endurance limit measured in air. Both, scatter range and grouping, will be focused on in future research activities.

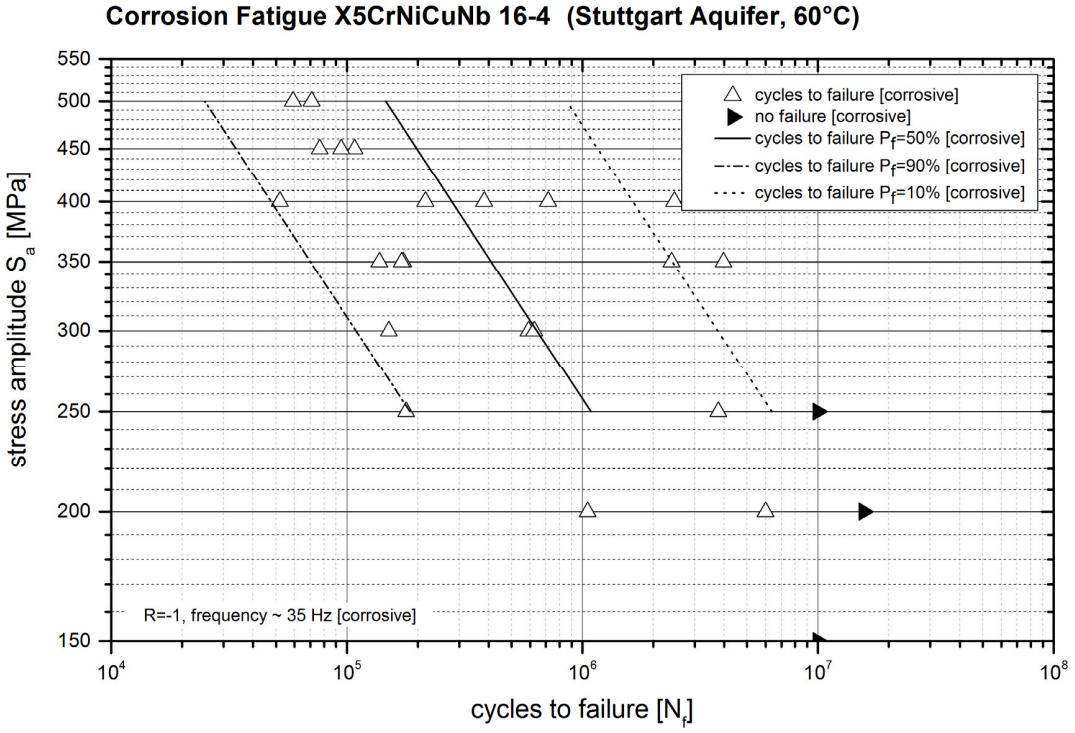


Fig. 8: S-N-curve and sample of 1.4542 exposed to flowing saline aquifer [20] and $CO_2$ at 60 °C.

For X46Cr13 localized corrosion (pit corrosion or pitting) is identified as the cause of failure [33] (figure 9, left). Local corrosion phenomena like shallow pit corrosion and pits of various dimensions lead to crack initiation under mechanical load. Pits are often only 0.1 mm deep and 0.2 mm wide. This distinct corrosive damage shows short cracks about 0.05 mm in the components that are transversal to the sample length. Opening and closing of the crack during cyclic load enhances local corrosion. Once the crack opens the crack flank surfaces corrode continuously during cyclic load. Cyclic loading of fatigue specimens in the same corrosive environment as the exposure specimens leads to a higher number of pits per unit area. Static experiments reveal an increase in number of pits after long exposure, but there is no such significant time dependence for the fatigue specimens. Therefore the stress amplitude $\sigma_a$ has little to no influence on the pit initiation: number of pits and fatigue life are not correlated.

Generally multiple cracks are found throughout the entire sample area of X5CrNiCuNb16-4 and not –as expected- only within the sample area that is mechanically loaded highest. Once the crack opens the crack-flank surfaces corrode continuously during cyclic load (figure 9). Crack propagation is then perpendicular to the direction of load. Localized corrosion (pits: 0.1 mm deep and 0.2 mm diameter) is accompanied with cracks, but not necessarily identified as the cause of crack initiation and failure under mechanical load.

In general pit formation on stainless steels is enhanced by chemical reactions, local changes of lattice energy within the steel`s surface and mechanical load. Within the microstructure an increase in dislocation number, grain boundaries, boundaries of precipitation phases e.g. carbides lead to local lattice mismatch resulting in higher local boundary energy [33]. This initiates local corrosion that may lead to crack formation and also accelerates crack propagation – both responsible for early failure.

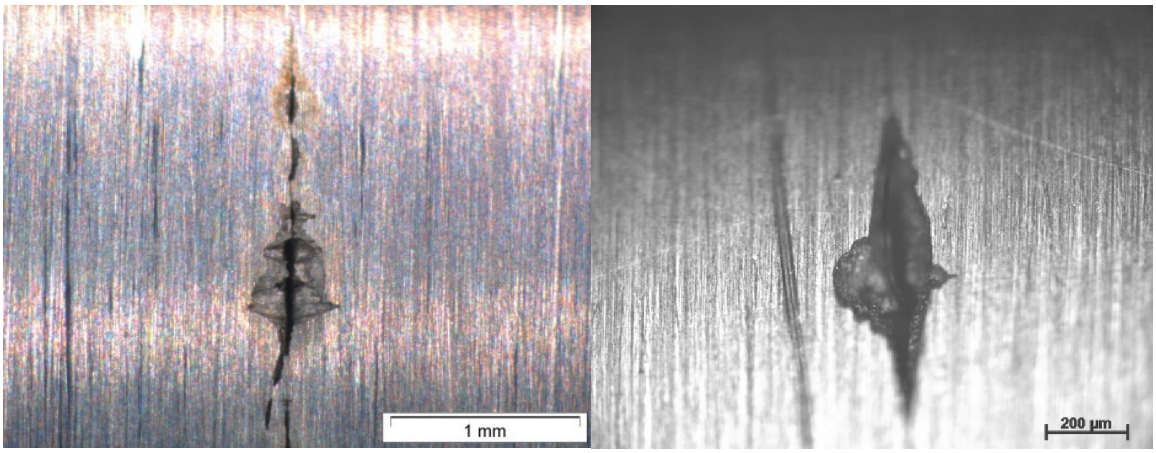


Fig. 9: Sample surfaces after testing (left: X46Cr13, right: X5CrNiCuNb16-4. Local corrosion leads to crack initiation and is most likely failure cause for X46Cr13.

Under corrosive conditions no typical endurance limit -as observed in S-N-curves from fatigue tests of in air- exists. The fatigue strength of the material in non-corrosive conditions of about 310 MPa for X46Cr13 and 340 MPa for X5CrNiCuNb16-4 is reduced significantly due to corrosion. Under these conditions the maximal number of cycles to failure observed was $1.10 \times 10^7$ at stress amplitude 173 MPa for X46Cr13 and $10 \times 10^6$ at a stress amplitude of 150 MPa for X5CrNiCuNb16-4. Crack formation is correlated with pit corrosion phenomena resulting in intercrystalline corrosion, but only for X46Cr13 failure is a consequence of local corrosion.

### *3.3. In-Situ Electrochemical Tests*

The samples were contained for three days in the reference test stand. This refers to the time of one fatigue test in the corrosion chamber with $10^7$ cycles. The results of the reference test stand show that the measured potential is identical with the initial potential in the corrosion chamber. Therefore the corrosion chamber set up does not influence the electrochemical measurements and the potential obtained during in-situ fatigue tests refer to the real results of the material tested.

The potential measured via reference test stand shows no particularly large changes. Potential measurements during fatigue tests show that cracking of the specimen is accompanied with a drop of the potential. Thus follows that both, mechanical load and the crack propagation are crucial for the potential change.

The potential of X5CrNiCuNb16-4 is at about 100 mV when measured versus an Ag / AgCl reference electrode. In general the potential drop was accompanied by the failure of the specimen. From the start until the end of the tests the potential changed about 100 mV (figure 10). For specimens which are not failure, the potential did not change much.

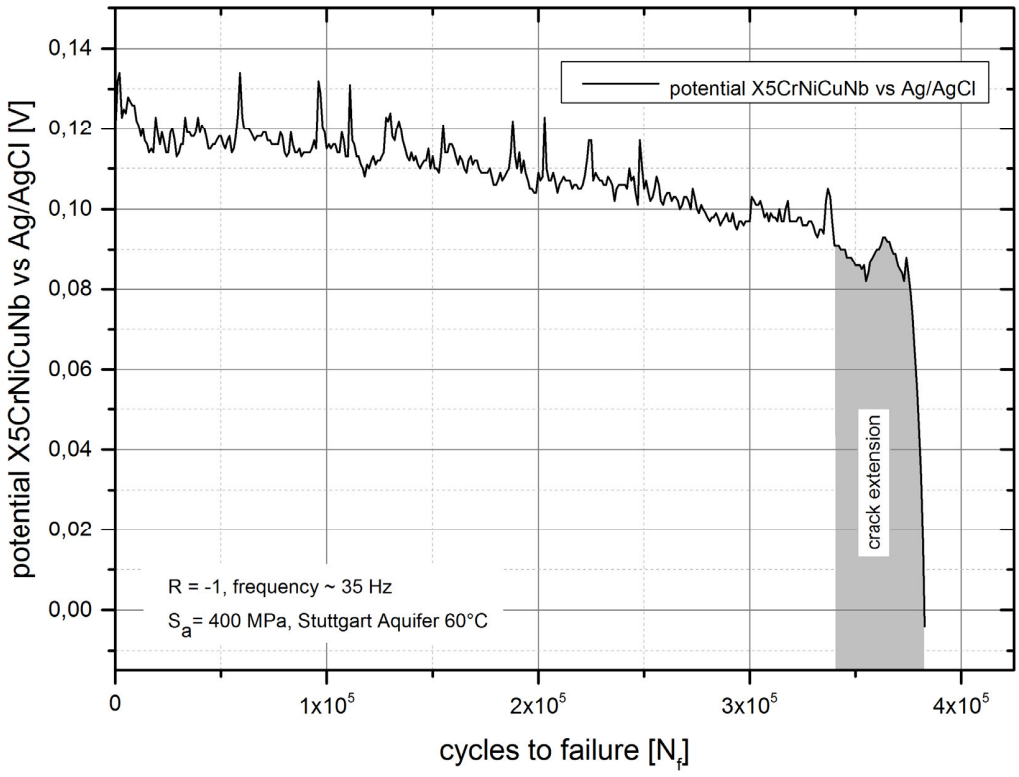


Fig. 10: Electrochemical Potential of X5CrNiCuNb16-4 versus Ag/AgCl electrode during fatigue tests.

## 4. Conclusion

Injection pipe steels with 13% Chromium and 0.46% Carbon (X46Cr13, 1.4034) or 0.05% Carbon (X5CrNiCuNb16-4, 1.4542) were differently heat treated and then exposed up to 8000 h (approximately 1 year) to $CO_2$ and saline aquifer water at ambient pressure as well as 100 bar and 60 °C in laboratory experiments. A highly flexible corrosion chamber allowing for electrochemical testing, $O_2$-partial pressure or gas partial pressure measurement was designed to support stress-strain loaded corrosion fatigue experiments by enabling an in-situ corrosive environment which may be used up to 100 °C at ambient pressure. To simulate non-static operation a resonant testing machine has been used at 30 – 40 Hz where samples of both steels were tested in stress-strain mode under CCS aquifer environment. In addition technical $CO_2$ was introduced into the closed system at a rate close to 9 L/h to keep stable environmental conditions.

Following findings are noteworthy:

- Non-uniform corrosion forms carbonate corrosion products on the surface such as siderite and goethite.
- Surface corrosion products on AISI630 (X5CrNiCuNb16-4, 1.4542) show rather unusual pattern which is possibly explained by the distinct microstructure of the steel
- For X46Cr13 localized corrosion (pit corrosion or pitting) is identified as the cause of failure [33].
- The scatter range TN = 1:34 of X5CrNiCuNb16-4 is disproportionately large compared to the scatter range of X46Cr13 (1:4). Localized corrosion is present, but identified as the cause of crack initiation and failure.

- The corrosion fatigue behaviour of AISI630 (X5CrNiCuNb16-4, 1.4542) is described by statistical crack initiation but characteristic crack propagation and fracture surfaces for one stress amplitude. A typical fatigue strength of the S-N-curve does not exist under CCS corrosive conditions. The fatigue strength of the material in non-corrosive conditions of under cyclic rotation of 620 MPa is reduced significantly due to corrosion. Note, that cyclic rotation does not accurately compare to compression-tension testing and that reference measurements are due in future experiments.
- The measured potential in the reference test stand is identical with the initial potential in the corrosion chamber.
- Fatigue tests show that cracking of the specimen is accompanied with a drop of the potential.

According to DIN 6601 both steels would be unsuitable for pressure vessel application, when being surrounded by the $CO_2$-saturated brine due to their susceptibility towards pitting. Even when surface corrosion rates are low, pit growth rates only allows the steel to be suitable for injection pipes in CCS environments if monitored closely.

## Acknowledgement

This work was supported by the FNK (Fachkonferenz für wissenschaftlichliche Nachwuchskräfte) of the Applied University of Berlin, HTW and by IMPACT (EU-Project EFRE 20072013 2/21).

## References

[1] Carvalho, D.S., Joia, C.J.B., Mattos, O.R., Corrosion rate of iron and iron-chromium alloys in $CO_2$-medium, Corrosion Science 47 (2005) 2974-2986.
[2] Thomas, D.C., Carbon Dioxide Capture for Storage in Deep Geologic Formations – Results from $CO_2$ Capture Project, Volume 1: Capture and Separation of Carbon Dioxide form Combustion Sources, $CO_2$ Capture Project, Elsevier Ltd UK 2005, ISBN 0080445748.
[3] Nešić, S., Key issues related to modelling of internal corrosion of oil and gas pipelines – A review, Corrosion Science 49 (2007) 4308–4338.
[4] Cui, Z.D., Wu, S.L., Zhu, S.L., Yang, X.J., Study on corrosion properties of pipelines in simulated produced water saturated with supercritical $CO_2$, Applied Surface Science 252 (2006) 2368-2374.
[5] Pfennig, Anja ; Phillip Zastrow ; Axel Kranzmann, Influence of heat treatment on the corrosion behaviour of stainless steels during $CO_2$-sequestration into saline aquifer, International Journal of Green House Gas Control (213) 213-224
[6] Pfennig, A., Kranzmann, A., Reliability of pipe steels with different amounts of C and Cr during onshore carbon dioxid injection, International Journal of Greenhouse Gas Control 5 (2011) 757–769.
[7] Wu, S.L., Cui, Z.D., Zhao, G.X., Yan, M.L., Zhu, S.L., Yang, X.J., EIS study of the surface film on the surface of carbon steel form supercritical carbon dioxide corrosion", Applied Surface Science 228 (2004) 17-25.
[8] Bilmes, P.D., Llorente, C.L., Méndez, C.M., Gervasi, C.A., Microstructure, heat treatment and pitting corrosion of 13CrNiMo plate and weld metals, Corrosion Science 51 (2009) 876-882.
[9] Bülbül, Ş., Sun, Y., Corrosion behaviours of high Cr-Ni cast steels in the HCl solution, Journal of Alloys and Compounds 598 (2010) 143-147.
[10] Cvijović Z., and Radenković, G., Microstructure and pitting corrosion resistance of annealed duplex stainless steel, Corrosion Science 48 (2006) 3887-3906.
[11] Hou, B. , Li, Y., Li, Y., Zhang, J., Effect of alloy elements on the anti-corrosion properties of low alloy steel, Bull. Mater. Sci. 23 (2000) 189-192.
[12] Zhang, L., Zhang, W., Jiang, Y., Deng, B., Sun, D., Li, J., Influence of annealing treatment on the corrosion resistance of lean duplex stainless steel 2101, Electrochimica Acta 54 (2009) 5387–5392.
[13] Choi, Y.-S., Kim, J.-G., Park, Y.-S., Park, J.-Y., Austenitzing treatment influence on the electrochemical corrosion behaviour of 0.3C-14Cr-3Mo martnesitic stainless steel, Materials Letters 61 (2007) 244-247
[14] Isfahany, A. N., Saghafian, H., Borhani, G., The effect of heat treatment on mechanical properties and corrosion behaviour of AISI420 martensitic stainless steel, Journal of Alloys and Compounds 509 (2011) 3931-3936
[15] Park, J.-Y., Park, Y.-S., The effects of heat-treatment parameters on corrosion resistance and phase transformation of 14Cr-3Mo martensitic stainless steel, Materials Science and Engineering A 449-451 (2007) 1131-1134
[16] Dyja, D., Stradomski, Z., Pirek, A., Microstructural and fracture analysis of aged cast duplex steel, Strength of Materials, Vol. 40, No. 1 (2008) 122-125
[17] Lucio-Garcia, M.A., Gonzalez-Rodrigueza, J.G., Casalesc, M., Martinezc, L., Chacon-Navaa, J.G., Neri-Floresa, M.A. and Martinez-Villafañea A., Effect of heat treatment on $H_2S$ corrosion of a micro-alloyed C–Mn steel, Corrosion Science 51 (2009) 2380-2386

[18] Banaś, J., Lelek-Borkowska, U., Mazurkiewicz, B., Solarski, W., Effect of $CO_2$ and $H_2S$ on the composition and stability of passive film on iron alloy in geothermal water, Electrochimica Acta 52 (2007) 5704-5714.
[19] Moreira, R.M., Franco, C.V., Joia, C.J.B.M., Giordana, S., Mattos, O.R., The effects of temperature and hydrodynamics on the $CO_2$ corrosion of 13Cr and 13Cr5Ni2Mo stainless steels in the presence of free acetic acid, Corrosion Science 46 (2004) 2987-3003.
[20] Förster, A., Norden, B., Zinck-Jørgensen, K., Frykman, P., Kulenkampff, J., Spangenberg, E., Erzinger, J., Zimmer, M., Kopp, J., Borm, G., Juhlin, C., Cosma, C., Hurter, S., 2006, Baseline characterization of the CO2SINK geological storage site at Ketzin, Germany: Environmental Geosciences, V. 13, No. 3 (September 2006), pp. 145-161.
[21] Seiersten, M., Material selection for separation, transportation and disposal of $CO_2$, Corrosion paper no. 01042 (2001).
[22] Choi, Y.-Y. and Nešić, S. Determining the corrosive potential of $CO_2$ transport pipline in high $pCO_2$-water environments, Journal of Green House Gas Control 5 (2011) 788-797.
[23] Han, J., Zhang, J., Carey, J.W., Effect of bicarbonate on corrosion of carbon steel in $CO_2$-saturated brines, Journal of Green House Gas Control 5 (2011) 1680-1683.
[24] Pfennig, A., Kranzmann, A., 2012, Effect of $CO_2$ and pressure on the stability of steels with different amounts of Chromium in saline water, Corrosion Science (2012) 441–452,
[25] Pfennig, A., Linke, B., Kranzmann, A. Corrosion behavior of pipe steels ex-posed for 2 years to $CO_2$-saturated saline aquifer environment similar to the CCS-site Ketzin, Germany, Energy Procedia, Vol. 4 (2011) 5122-5129.
[26] Mu, L.J. Zhao, W.Z., Investigation on carbon dioxide corrosion behavior of HP13Cr110 stainless steel in simulated stratum water, Corrosion Science 52 (2010) 82-89.
[27] Giese, L.B. et al: Geochemie der Formationsfluide der Bohrung E Groß Schönebeck 3/90, STR02/14, Geothermie Report 02-1 (2001) 145 – 169
[28] Thomas, J.P. and Wei, R.P., Corrosion fatigue crack growth of steels in aqueous solutions I: Experimental results and modeling the effects of frequency and temperature, Material Science and Engineering, A159 (1992) 205-221
[29] Unigovski, Ya.B., Lothongkum, G., Gutman, E.M., Alush, D., Cohen, R., Low-cycle fatigue behaviour of 316L-type stainless stell in chloride solutions, Corrosion Science 51 (2009) 3014-3120
[30] C.M. Holtam, D.P. Baxter, I.A. Ashcroft, R.C. Thomsen, Effect of crack depth on fatigue crack growth rates for a C-Mn pipeline steel in a sour environment, International Journal of Fatigue 32 (2010) 288-296
[31] Thorbjörnsson, I., Corrosion fatigue testing of eight different steels in an Icelandic geothermal environment, Materials and Design Vol.16 No. 2 (1995) 97-102
[32] Roeder, E., Bassler, H.-J., Huber M. und Vollmar, J., Schwingungsrisskorrosionsverhalten des austenitischen Stahles X6CrNiMoTi 17 12 2 in 3%iger NaCl-Lösung unter Umlaufbiegebelastung, Werkstoffe und Korrosion 43 (1992) 426-431
[33] Pfennig, A., Wiegand, R., Wolf, M., Bork, C.-P., Corrosion and corrosion fatigue of AISI 420C (X46Cr13) at 60 °C in $CO_2$-saturated artificial geothermal brine, Corrosion Science 68 (2013) 134–143